HHS Public Access

Author manuscript

ACS Appl Mater Interfaces. Author manuscript; available in PMC 2019 October 03.

Published in final edited form as:

ACS Appl Mater Interfaces. 2018 October 03; 10(39): 33464–33473. doi:10.1021/acsami.8b11974.

P-glycoprotein-Targeted Photothermal Therapy of Drug-Resistant Cancer Cells using Antibody-Conjugated Carbon Nanotubes

Xubin Suo[1,2], **Brittany N. Eldridge**[1], **Han Zhang**[1,3], **Chengqiong Mao**[1], **Yuanzeng Min**[4], **Yao Sun**[5], **Ravi Singh**[1,*], and **Xin Ming**[1,6,*]

[1]Department of Cancer Biology, Wake Forest University School of Medicine, Winston Salem, North Carolina, United States;

[2]School of Pharmacy, Guangdong Pharmaceutical University, Guangzhou, Guangdong, China;

[3]School of Traditional Chinese Medicine, Guangdong Pharmaceutical University, Guangzhou, China;

[4]Department of Chemistry, University of Science and Technology of China, Hefei, Anhui, China;

[5]Department of Radiology, Wake Forest University School of Medicine, Winston Salem, North Carolina, United States;

[6]Department of Biomedical Engineering, Wake Forest University School of Medicine, Winston Salem, North Carolina, United States.

Abstract

P-glycoprotein (Pgp)-medicated multidrug resistance (MDR) remains a formidable challenge to cancer therapy. As conventional approaches using small-molecule inhibitors failed in clinical development because of the lack of cancer specificity, we develop Pgp-targeted carbon nanotubes to achieve highly cancer-specific therapy through combining antibody-based cancer targeting and locoregional tumor ablation with photothermal therapy. Through a dense coating with phospholipid-poly(ethylene glycol), we have engineered multiwalled carbon nanotubes (MWCNTs) which show minimum nonspecific cell interactions and maximum intercellular diffusion. After chemically modified with an anti-Pgp antibody, these MWCNTs showed highly Pgp-specific cellular uptake. Treatment of the targeted MWCNTs caused dramatic cytotoxicity in MDR cancer cells upon photoirradiation, whereas they did not cause any toxicity in the dark or phototoxicity toward normal cells that do not express Pgp. Because of excellent intratumor diffusion and Pgp-specific cellular uptake, the targeted MWCNTs produced strong phototoxicity in tumor spheroids of MDR cancer cells, a 3-D tumor model for studying tumor penetration and therapy. In conclusion, we have developed a highly Pgp-specific MWCNTs that may provide an effective therapy for MDR cancers where other approaches have failed.

[*]Corresponding authors: Xin Ming (xming@wakehealth.edu) and Ravi Singh (rasingh@wakehealth.edu).

Conflicts of interest

There are no conflicts to declare.

Supporting Information

Effect of nanotube diameter on photothermal heating and UV-Vis-NIR spectra of the nanotubes supplied as Supporting Information.

Graphical Abstract

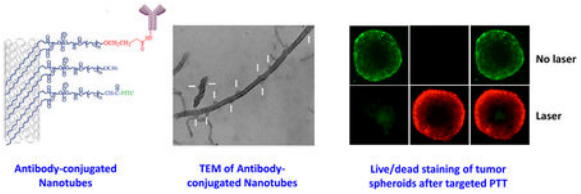

Keywords

Cancer multidrug resistance; Cancer targeting; Carbon nanotubes; P-glycoprotein; Photothermal therapy

Introduction

The development of drug resistance causes failure for the treatment of patients with metastatic cancers. Increased expression of P-glycoprotein (Pgp), an ATP-binding cassette transporter, is considered as a leading cause of cancer drug resistance.[1] Chemotherapy agents, including doxorubicin and taxol, achieve their anticancer actions only after they enter cancer cells. Pgp is expressed on the surface membrane of cancer cells, and mediates efflux of many of these agents, which are its substrates. Thereafter, drug resistance arises in these cancer cells because of the overexpression of Pgp. Although its role in cancer drug resistance was discovered over three decades ago, Pgp is still an undruggable target, and no clinical solution exists to overcome this resistance. Three generations of small-molecule inhibitors have been developed to overcome Pgp-medicated drug resistance, yet none of them have been approved by the US Food and Drug Administration.[1] The main reason for this failure is the lack of cancer specificity of these inhibitors, which caused side effects in normal tissues.[2]

Increased cancer specificity can be achieved using photothermal therapy (PTT) through locoregional tumor ablation. This emerging treatment modality employs laser emitted near-infrared (NIR) radiation to heat malignant tissue to temperatures in excess of 50°C, which causes protein denaturation, aggregation and oxidation, and ultimately cell death.[3] Because of its precise energy delivery to target cells and the sensitivity of cancer cells to temperature elevation, PTT has been widely investigated as a noninvasive treatment approach for recurrent or drug-resistant cancers.[4] Although laser-based therapy results in few side effects,[5–8] the inability to achieve sufficiently high temperatures evenly throughout the target lesion limits its clinical application.[9] To address this issue, nanomaterials including carbon nanotubes (CNTs)[10] and gold nanoparticles (NPs)[11–14] have been intensively investigated for their capacity to generate heat in response to NIR exposure.[15] CNTs, which were first described by Ijima et al.,[16] are a heterogeneous class of nanomaterials that consist of sheets of sp^2 carbon rolled into single-walled or multiwalled tubes. In addition to PTT, potential biomedical applications of CNTs include drug and gene delivery,[17–18] and radionuclide delivery for noninvasive imaging.[19–21] CNT-mediated PTT allows far greater heat deposition and localization within a target tumor than laser irradiation alone,[9,22–26] and is effective for treating bulk tumor and stem cell-like cancer cell population that is believed to be

responsible for the development of therapeutic resistance and disease recurrence.[27–28] In general, PTT using multiwalled CNTs (MWCNTs) has proven to be more effective than single-walled CNTs (SWCNTs) for heat generation and localization.[10] PTT using gold NPs also has been widely investigated,[11–14] but gold NPs can become deformed following heating, which reduces the efficacy of subsequent heating cycles.[29] In contrast, CNTs do not deform after NIR exposure, allowing multiple heat cycles without loss of efficacy.[23]

Despite the significant potential for cancer cell-specific killing, NP-mediated PTT has thus far failed to deliver on the hope for improvements during ongoing clinical trials.[30] A significant obstacle for achieving this goal is the fact that most NPs fail to diffuse throughout tumors and are trapped by the extracellular matrix, leading to heterogeneity in their intratumoral distribution, even after local delivery.[31] However, the intercellular diffusion rate of nanotubes is anomalously high in comparison to globular particles with similar weight, and is comparable to molecules with molecular weights 10,000-fold lower.[32] This is because CNTs possess a high aspect ratio which allows them to align along their narrow axis and pass through small pores that may restrict the passage of globular macromolecules of similar mass.

One advantage of using NPs for cancer therapy is the capacity to engineer them to selectively bind to receptors expressed on target cells. There are several reports indicating that increased uptake of CNTs by cancer cells can be achieved through conjugation of targeting moieties to the surface of CNTs. This strategy is versatile and CNTs have been targeted to cell receptors including the folate receptor,[26,33] HER2,[34–35] glucose transporters,[21] a carbohydrate antigen overexpressed in neuroblastomas,[36] integrins,[37] and CD133.[27] In each case, these ligands bind to the targeted membrane proteins that are overexpressed in tumors. Because Pgp is a membrane transporter that is overexpressed in many tumors, and Pgp-expressing cancer cells are resistant to conventional chemotherapy, Pgp-targeted PTT may provide a means to overcome cancer resistance and treat these difficult cancers in a more specific way than small-molecule inhibitors.

In this study, we aimed to provide a highly cancer-specific approach to Pgp-overexpressing cancers by combining antibody-based cancer targeting and locoregional tumor ablation with PTT. Thus, MWCNTs were conjugated to a Pgp-specific antibody (Pab). After physicochemical characterization of the targeted NPs, we examined their cellular uptake and phototoxicity in Pgp-expressing cancer cells. We further investigated the mechanism of phototoxicity caused by the targeted MWCNTs, and evaluated their anticancer actions in 3-D tumor spheroids of drug-resistant cancer cells.

Experimental Section

Chemicals and Reagents

Short oxidized MWCNTs with 0.5–2 μm in length and in three diameters (<8 nm; 8–15 nm; 20–30 nm) were purchased from Nanostructured and Amorphous Materials. Distearoyl-*sn*-glycero-3- phosphoethanolamine conjugated to polyethylene glycol$_{5000}$ terminated with a methoxy group (DSPE-PEG), maleimide (DSPE-PEG-Mal), and fluorescein isothiocyanate (DSPE-PEG-FITC) were purchased from Nanocs, Inc. N-Succinimidyl S-acetylthioacetate

(SATA) and hydroxylamine hydrochloride were purchase from Thermo Scientific. Ethylenediaminetetraacetic acid disodium salt dehydrate, sodium hydroxide solution, penicillin and streptomycin were obtained from Sigma-Aldrich. An anti-Pgp monoclonal antibody (15D3) was produced in house using a method described previously.[38] Water used in all experiments was purified using a Milli-Q water purification system (Millipore, S.A.S, B.P).

Preparation of Pab-MWCNTs

To reduce size and increase aqueous dispersibility, the initial stock of MWCNTs was further acid oxidized using sulfuric acid and nitric acid (3:1 mixture) treatment followed by extensive washing and purification as previously described.[21,39] Subsequently, Pab-MWCNTs were prepared according to Scheme 1. Briefly, DSPE-PEG (50 mg), DSPE-PEG-Mal (40 mg), and DSPE-PEG-FITC (10 mg) were dissolved in 5 mL of water, and then added into a glass vial containing 20 mg of MWCNTs treated as described above. The resulting mixture was dispersed by bath sonication six times for 10 min, with exchanging water between cycles to prevent overheating as previously described.[39,40] The coated MWCNTs were washed four times in 20 mL of water using size exclusion columns (100K MWCO, Millipore) to remove any excess phospholipids. The concentration of MWCNTs in the final solution was estimated to be 4 mg/mL based upon UV/vis absorbance in comparison to a standard curve of the starting material.

To prepare Pab-MWCNTs, the Pgp antibody was first conjugated with SATA (Thermo Scientific) in phosphate buffered saline (PBS) (pH 7.4) at the ratio of antibody to SATA of 1:5, and then was deacetylated with 50 mM hydroxylamine to generate sulfhydryl groups after purification. The MWCNTs-PEG-Mal suspension (4 mg/mL MWCNTs in 1.0 mL of PBS, pH 7.4) was reacted with the freshly made thiolated Pgp antibody (1 mg/mL in 0.5 mL of PBS). The reaction was performed for 3 h at room temperature under magnetic stirring. The Pab-MWCNTs were stored in PBS at 4°C until ready for use.

Conjugation of antibodies to MWCNTs and reaction completion were confirmed using a modified dot blot technique. Briefly, solutions of the thiolated Pgp antibody alone, MWCNT-PEG-Mal, Pab-MWCNT, and a mixture of the Pgp antibody with MWCNT-PEG (Pgp antibody concentration was the same in all samples) were diluted 40-fold in PBS and were centrifuged at 30,000 × g. The Pgp antibody was quantified by placing 10 μL of the supernatant on a nitrocellulose membrane (Thermo Scientific) and dried overnight. The membrane was rocked for 1 h at room temperature in Tris-buffered saline containing 5% powdered milk, 1% triton X-100, and a 1:1000 dilution of horse radish peroxidase conjugated, polyclonal anti-mouse IgG (Cell Signaling Technologies). After washing, immunoreactive products were visualized by chemiluminescence (SuperSignal Femto West, Thermo-Fisher).

Characterization of Pab-MWCNTs

The morphology of Pab-MWCNTs was imaged using a FEI Tecnai Spirit transmission electron microscope equipped with a digital imaging system. In this experiment, a dilute suspension of MWCNTs or Pab-MWCNTs was dried on a 200 mesh carbon coated copper

grid. A second set of samples were similarly prepared and then were negatively stained using 1% uranyl acetate in water. The MWCNTs were imaged by transmission electron microscopy (TEM) at an accelerating potential of 80 keV. The length, diameter, and aspect ratio (length/diameter) of the MWCNTs were quantified manually from the TEM images using Image J (https://imagej.nih.gov/ij/). At least 100 MWCNTs were analyzed from each group. Further, the hydrodynamic diameter of MWCNTs was assessed by dynamic light scattering using Malvern Zetasizer NS90 in PBS in automatic mode. The ζ-potential of MWCNTs was assessed in Milli-Q water at pH 6.8–7 using Malvern Zetasizer NS90.

Cell Culture

The cell line 3T3-MDR1 is a mouse fibroblast cell line stably transfected with a cDNA coding for human Pgp and was obtained from Dr. Gottesman's lab at National Cancer Institute (NCI). This cell line was maintained in the Dulbecco's modified Eagle's medium (DMEM) (Corning, NY, USA) supplemented with 10% fetal bovine serum (FBS, Sigma-Aldrich), 400 IU/mL penicillin, 100 μg/mL streptomycin (Corning, NY, USA), and 60 ng/mL colchicine (Sigma-Aldrich). The 3T3 control cells were obtained from ATCC (Manassas, VA, USA), and were maintained in the DMEM cell culture medium supplemented with 10% FBS, 400 IU/mL penicillin, and 100 μg/mL streptomycin. NCI/ADR-RES is an adriamycin-resistant ovarian cancer (OvCa) cell line with the high expression level of Pgp,[38] and was also obtained from NCI. It was maintained under the same conditions as the 3T3-MDR1 cell line.

Cellular Uptake of Pab-MWCNTs

To examine the Pgp-specific uptake of Pab-MWCNTs, 3T3 and 3T3-MDR1 cells were seeded in 24-well plates at a density of 1×10^5 cells/well. The cells were allowed to adhere overnight, and then were treated with FITC-labelled Pab-MWCNTs or MWCNTs (10 μg/mL of MWCNTs). After incubation for 1, 4, and 24 h, the cells were washed with PBS twice and digested with trypsin. The FITC fluorescence of cells was then detected by flow cytometry using a FACS Canto II cytometer (BD, Franklin Lakes, NJ, USA). Cellular uptake of FITC-labelled Pab-MWCNTs was also examined by confocal microscopy. The 3T3 and 3T3-MDR1 cells were seeded in a glass bottom chamber and were cultured overnight. The cells were exposed to FITC labelled Pab-MWCNTs (10 μg/mL of MWCNTs) for 4 h. The cells were then washed with PBS twice, and imaged by Olympus FV1200 confocal microscopy (Olympus, Tokyo, Japan).

Phototoxicity of Pab-MWCNTs

To examine the Pgp-specific killing of Pab-MWCNTs, 3T3 and 3T3-MDR1 cells (1×10^5 cells/well) were seeded in 24-well plates. The cells were allowed to adhere overnight, and then were treated with Pab-MWCNTs or MWCNTs at different concentrations for 1 h. After washing, the cells were irradiated with a K-laser (K-LASER, Franklin, TN, USA) at a wavelength of 970 nm and an irradiance of 6 W/cm^2 for 45 s. After culturing overnight, the viability of the cells was determined using the Alamar Blue assay as described previously.[41,42] The phototoxicity of the targeted and control NPs was also examined with live/dead cell staining. After NP treatment and laser irradiation, the cells were co-stained with Calcein

AM (2 μM) and propidium iodide (PI, 5 μg/mL) at room temperature for 30 min, rinsed with PBS, and then imaged using a Cytation 5 Imaging Reader (BioTek, Winooski, VT, USA).

Flow Cytometric Analysis of Phototoxicity

NCI/ADR-RES cells were treated with Pab-MWCNTs, and then irradiated with the K-laser as described above. At 10 min, 4 h, and 24 h post irradiation, the cells were trypsinized, washed twice, and stained with APC labeled Annexin V and PI (BD) according to the manufacturer's instruction. The fluorescence of the stained cells was detected with a BD FACS Canto II flow cytometer.

Phototoxicity of Pab-MWCNTs in Tumor Spheroids

For spheroid generation, NCI/ADR-RES cells were seeded in ultra-low attachment 96-well round-bottomed plates (Thermo Fisher Scientific) at a density of 8000 cells in 200 μL media per well and cultured for 4 days. The spheroids were divided into 3 groups with 20 spheroids in each group. The first group of spheroids was exposed to Pab-MWCNTs at final concentration of 25 μg/mL for 1 h. The second group was treated with nontargeted MWCNTs at the same concentrations, and the last group was not treated with NPs. The spheroids were then washed with fresh media three times. Half spheroids in each group were then irradiated with the K-laser (970 nm; 6 W/cm^2; 45 s). After 1 day, some tumor spheroids were stained with Calcein AM and PI for live/dead cell staining, whereas others were stained with the Alamar Blue reagent to quantify the viability. The remaining spheroids were imaged daily using the Cytation 5 Imaging Reader to estimate their growth over a week.

Statistical Analysis

Quantitative data are expressed as mean ± SD. They were compared using Student's *t*-test for two sample comparison or one-way ANOVA followed by Tukey's post-hoc analysis for multiple comparisons. *P* values < 0.05 were considered statistically significant.

Results

Characterization of Pab-MWCNTs

We initially determined the photothermal heating efficiency following laser irradiation (970 nm; 3 W; 30 s) of aqueous dispersions of acid oxidized SWCNTs and MWCNTs with increasing diameters (<8 nm; 8–15 nm; 20–30 nm). As shown in Figure S1, SWCNTs were significantly less efficient at photothermal heating than MWCNTs, and heat generation per unit mass increased as a function of both nanotube concentration and diameter. However, MWCNT toxicity is also reported to increase with diameter.[43] Therefore, although the 20–30 nm diameter MWCNTs generated the most heat per unit mass of the materials tested, we selected 8–15 nm diameter MWCNTs for further testing.

To achieve cancer-specific targeting, it is necessary not only to introduce a targeting moiety, but also to minimize nonspecific interactions that could reduce selectivity. Notably, we recently found that acid oxidation and coating MWCNTs using a 2 w/v% solution of DSPE-PEG, which is twice what is typically used to disperse CNTs,[40] reduces nonspecific cell uptake at least 6-fold compared to uncoated MWCNTs without any loss of heat transduction

capability, and dramatically increases their diffusion through extracellular space.[39] When prepared in this manner, MWCNTs diffuse over centimeter length distances. In contrast, uncoated MWCNTs and MWCNTs coated in lower concentrations of surfactants remained within a few millimeters of the infusion site.[39] Furthermore, we showed that similarly functionalized MWCNTs were not thrombogenic following intravenous administration in mice,[44] and we and others demonstrated that DSPE-PEG coated MWCNTs accumulate in tumors in mice.[10,21,37]

Building on these studies, we coated 8–15 nm diameter MWCNTs with a 2 w/v% solution of a mixture of DSPE-PEG, DSPE-PEG-Mal, and DSPE-PEG-FITC at a 5:4:1 mass ratio, and then conjugated to Pgp antibodies (Pab) to generate Pab-MWCNTs according to the procedures shown in Scheme 1. Non-targeted MWCNTs (hereafter referred to only as MWCNTs) were coated with a 9:1 mass ratio mixture of DSPE-PEG and DSPE-PEG-FITC. Size distribution and binding of Pab to MWCNTs initially was assessed by TEM (Figure 1A–F). As shown in Figure 1A, D, the median length and width of the MWCNTs used in this study was less than 200 nm and less than 11 nm, respectively, and these characteristics were not significantly altered following conjugation to Pab. At higher magnification (Figure 1B, E), distinct differences can be observed between the morphology of MWCNTs and Pab-MWCNTs. Compared with MWCNTs, there were spherical masses about 16 nm in diameter found in close proximity to the surface of the MWCNTs. On the basis of a previous report[45] and our estimation of the TEM images, it is likely that there are 10–12 antibodies bound to a carbon nanotube. The high density of Pab coating on MWCNTs is even more apparent in negatively-stained (uranyl acetate) TEM images (Figure 1C, F).

We further confirmed conjugation of antibodies to MWCNTs and reaction completion using a modified dot blot technique. Figure 1G shows the results of immunoblotting to probe for the presence of the Pab antibody with the anti-mouse secondary antibody in the supernatants of solutions containing Pab alone, MWCNT alone, freshly prepared Pab-MWCNT, and a mixture of Pab with MWCNT (Pab concentration was the same in all samples) after they were centrifuged at 14,000 × g to precipitate MWCNTs. Pab remained in the supernatant after centrifugation of Pab alone or Pab mixed with MWCNTs, but was not detected in the Pab-MWCNT or MWCNT alone samples. This indicated that all Pab in the reaction mixture was conjugated to MWCNTs, with little nonspecific binding.

We further characterized the colloidal stability of Pab-MWCNT dispersed in PBS, pH 7.4 (Figure 1H). After conjugation with the antibody, the hydrodynamic size of the nanotubes increased from 142.5 ± 0.6 to 217.6 ± 4.7 nm. No size increase was observed by TEM, and it is likely that this increase is because of the antibodies on the end of the PEG chain extending away from the MWCNT surface leading to increased drag in the solution. We also noted a significant change in the ζ-potential in water (pH 6.5), which was −55.1 ± 2.6 mV for MWCNTs and −18 ± 1.4 mV for Pab-MWCNTs because of the presence of the antibody. Both Pab-MWCNTs and unconjugated MWCNTs remained stably suspended without evidence of aggregation in PBS for at least a month at room temperature (data not shown). We measured UV-vis-NIR spectra of MWCNT and Pab-MWCNT. As shown in Figure S2, both nanotubes possess an extremely broad absorbance spectrum, covering the full spectra of NIR windows.

Cellular uptake of Pab-MWCNTs

Cellular uptake of FITC labelled Pab-MWCNTs was assessed in 3T3 and 3T3-MDR1 cells using flow cytometry. As shown in Figure 2A, the cellular uptake of Pab-MWCNTs by 3T3-MDR1 cells was much greater than that by 3T3 cells at all time points. Recent studies have shown that internalization of CNTs greatly increases the efficacy of PTT in comparison to treatment of cells with nanotubes bound to their surface.[34,46] Although Pgp is thought of as a cell membrane protein, recent studies have established that it is routinely endocytosed from the plasma membrane and brought into the cell, thus remaining active in lysosomes.[47] Therefore, we examined the internalization of Pab-MWCNTs by confocal fluorescence microscopy. The FITC-labelled Pab-MWCNTs showed substantially more cellular uptake in 3T3-MDR cells than in 3T3 cells (Figure 2B), confirming Pgp-specific uptake of Pab-MWCNTs. In addition, the majority of the NPs were observed in the intracellular vesicles of 3T3-MDR cells (Figure 2B), and therefore it is likely that endocytosis was the major cellular uptake pathway of Pab-MWCNTs. These results indicated that the cellular uptake of Pab-MWCNTs was dependent upon the presence of Pgp on the cell surface.

Phototoxicity of Pab-MWCNTs

The selectivity and dose-dependent phototoxicity of MWCNTs and Pab-MWCNTs were examined in 3T3 and 3T3-MDR cells using the Alamar Blue assay. For this experiment, all cells were exposed to identical NIR laser irradiation (970 nm; 6 W/cm^2; 45 s) after the treatment of Pab-MWCNTs or nontargeted MWCNTs, respectively. As shown in Figure 3A, Pab-MWCNTs produced dose-dependent photokilling of 3T3-MDR1 cells but did not hurt the control 3T3 cells after laser irradiation, indicating the Pgp-specific phototoxicity of Pab-MWCNTs. MWCNTs alone did not produce phototoxicity to both 3T3 and 3T3-MDR1 cells. Neither Pab-MWCNTs nor nontargeted MWCNTs were cytotoxic to either the cell line in the absence of laser irradiation (Figure 3A). The results of live/dead cell staining shown in Figure 3B confirmed Pgp-specific photokilling of Pab-MWCNTs. About half of the 3T3-MDR1 cells were killed immediately by Pab-MWCNTs mediated PTT, whereas this treatment did not cause cell death in 3T3 cells (Figure 3B).

The Pgp-specific photokilling of Pab-MWCNTs was also examined in a drug-resistant cancer cell line NCI/ADR-RES. Similar to 3T3-MDR1 cells, the majority of NCI/ADR-RES cells were killed by Pab-MWCNT-mediated PTT, whereas nontargeted MWCNT treatment followed by laser irradiation did not cause cell death (Figure 4), indicating that Pab-MWCNTs mediated PTT produces Pgp-specific phototoxicity toward Pgp-expressing drug-resistant cancer cells.

Flow Cytometric Analysis of Phototoxicity of Pab-MWCNTs

The mechanism of cell death induced by Pab-MWCNTs mediated PTT was examined by Annexin V (AnV) and PI staining followed by time-lapse examination using flow cytometry to differentiate among the viable (AnV^-/PI^-; lower left quadrant), early apoptotic (AnV^+/PI^-; lower right quadrant), necrotic (AnV^-/PI^+; upper left quadrant), and late apoptotic/secondary necrotic (AnV^+/PI^+; upper right quadrant) cells. Apoptosis can be differentiated from necrosis based upon how cells progress to the late apoptotic/secondary necrotic stage. If the cells first pass through the early apoptosis prior to entering the late apoptotic/

secondary necrotic state, this will support an apoptotic cell death mechanism. If the cells proceed through necrosis to secondary necrosis, this will support a necrotic cell death mechanism. Analysis of the data in Figure 5 indicates a steady increase in late apoptotic/secondary necrotic cells (6.9%, 12.5%, and 19.6% at 10 min, 4 and 24 h post photoirradiation, respectively). Because cells first passed through either the early apoptosis or necrosis, indicating that both apoptosis and necrosis contributed to the cell death caused by Pab-MWCNT mediated PTT.

Phototoxicity of Pab-MWCNTs in Tumor Spheroids

Cell monolayers are a valuable tool for initial examination of the efficacy of novel cancer therapies, but the cells grown in a monolayer lack the complex interactions between the cells organized into a tissue, which can affect the response of cancer cells to photothermal treatment[39,48] and other cancer therapies.[49] In addition, cell monolayers lack the ability to mimic barriers to NP delivery such as diffusion through extracellular space. We and others have shown that properly functionalized MWCNTs can penetrate deeply within tumor spheroids.[32,39] Therefore, we evaluated the effects of Pab-MWCNT mediated PTT on multicellular, NCI/ADR-RES tumor spheroids.

The NCI/ADR-RES spheroids were treated with Pab-MWCNTs or nontargeted MWCNTs, for 1 h and then were irradiated with an NIR laser. After culturing overnight, some spheroids from each group were stained with Calcein AM (live stain) and PI (dead stain) and imaged using a Cytation 5 Imaging Reader. The results are shown in Figure 6A, from which we can see that Pab-MWCNTs plus laser group showed significant cell death when compared with control and MWCNT groups (laser or no laser). The untreated group (no laser) showed the highest cell viabilities. Quantitative viability assessment using the Alamar Blue assay confirmed the results from the live/dead cell staining assay. Only the treatment of Pab-MWCNTs followed by laser irradiation produced dramatic toxicity toward NCI/ADR-RES tumor spheroids (Figure 6B).

In parallel, the spheroid size was monitored before and after each treatment. As shown in Figure 6C, there was no obvious difference among the six groups before laser irradiation. One day after laser irradiation of both the Pab-MWCNT and nontargeted MWCNT groups, there was a slight physical inflation of the spheroids. On subsequent days, shrinking of the spheroid was apparent. However, by day 11 post-irradiation, the nontargeted MWCNT plus laser treated spheroids increased in size, whereas the Pab-MWCNT plus laser group did not. The spheroids treated without laser irradiation but with Pab-MWCNTs or MWCNTs continued to grow throughout the study. The untreated (no MWCNTs) spheroids continued to grow regardless of laser irradiation, and reached the largest physical sizes at the end of the study.

Discussion

Pgp-mediated drug resistance is a major cause for the failure of cancer chemotherapy. Although this mechanism has been known for over three decades and intensive efforts have been made to overcome this resistance, Pgp is still an undruggable target. The main hurdle for the conventional approaches, notably small-molecule inhibitors, is toxicity caused by

inhibiting Pgp in normal tissues, where it plays an important physiological role. The key for Pgp-targeted therapeutics is to limit the actions to the target cancer cells in the tumor site. Antibody-based drug targeting can enhance cancer specificity compared to the small-molecule approach; however, it cannot solve the problem completely as the anti-Pgp antibody still binds to the target in some normal tissues such as endothelial cells that form the blood-brain barrier. In this study, we combine antibody targeting with a laser-guided thermal therapy to achieve higher cancer specificity. Thus, we linked MWCNTs with the Pgp antibody, and examined the phototoxicity of Pab-MWCNTs in Pgp transfected 3T3 cells and Pgp-expressing drug-resistant cancer cells. The results indicated that Pab-MWCNTs specifically bound to 3T3-MDR1 cells (Figure 2), did not cause cytotoxicity in the absence of laser irradiation, but killed the targeted cells following brief exposure to NIR (Figures 3 and 4). Notably, Pab-MWCNTs did not bind to control 3T3 cells, which do not express Pgp, and following exposure to NIR, Pab-MWCNTs did not hurt 3T3 cells (Figure 3). Under similar conditions, neither nontargeted MWCNTs nor laser irradiation alone caused cell death. These results indicate that the phototoxicity of Pab-MWCNTs depends on two actions: (1) Pgp-mediated cellular binding/uptake of Pab-MWCNTs; (2) laser irradiation. The dual targeting properties of our Pgp-targeted PPT approach will reduce side-effects in normal tissues.

PTT causes cancer cell death via multiple mechanisms including apoptosis and necrosis, and the relative contributions of each mechanism depend on the localization of heat production.[28,50] In our flow cytometric analysis of cell death upon Pab-MWCNT mediated PTT, we observed both apoptotic and necrotic cell population (Figure 5), indicating both pathways contribute to the overall cell death of drug-resistant cancer cells. Confocal imaging showed that the Pab-MWCNTs both bind to the cell surface and are delivered into the cells and distributed throughout the intracellular compartments (Figure 2). The intense, nanoscale heat generated by NIR-stimulation of MWCNTs causes critical damage to adjacent membranes and organelles. Thus, intracellular damage near the perinuclear region may contribute to apoptotic cell death,[50] whereas damage close to the plasma membrane may cause direct cell necrosis.[28] The observation is consistent with a recent study indicating that apoptosis and other death pathways contribute to gold nanorods-based PTT of tumor xenografts in mice.[51]

The Pab-MWCNTs produced dramatic cancer cell death in tumor spheroids of Pgp-expressing, drug-resistant cancer cells (Figure 6). Tumor spheroids in 3D culture have been considered to be a better model to evaluate cancer therapy because they recapitulate some key features of the tumor microenvironment, including hypoxia and the presence of ECM.[52–54] These properties provide significant barriers to cancer responses to NP-based PTT. For example, the nanotubes need to sufficiently penetrate the tumor spheroids to selectively kill the majority of the cancer cells. Notably, we observed that Pab-MWCNTs combined with PTT were far more effective than nontargeted MWCNTs at inducing cell death in Pgp-expressing tumor spheroids. The high degree of cell death throughout the tumor spheroids caused by Pgp-targeted MWCNTs may indicate that: (1) Pab-MWCNTs have better penetration than nontargeted NPs in tumor spheroids; (2) binding of Pab-MWCNTs to tumors cells increases their retention within the spheroid; or (3) increased binding and uptake of Pab-MWCNTs further localizes nanoscale heating to vulnerable cell structures including membranes and organelles. Regardless of the specific underlying reasons, this

observation is consistent with our previous studies showing that targeted NPs have superior tumor penetration and therapeutic outcomes when compared to nontargeted NPs used for treatment of tumor spheroids.[41,42,55,56] Tumor spheroids often have a hypoxic core which provides another challenge for oxygen-dependent therapy, such as photodynamic therapy. As PTT does not depend on oxygen, this may contribute to its effective anticancer actions even in hypoxic regions in solid tumors.

We performed our studies using a 970 nm diode laser, but MWCNTs are broad absorbers across the NIR spectrum (Figure S2). Although there is a local maximum for water absorbance near 970 nm, the overall absorbance is low. Furthermore, absorbance by melanin and deoxygenated hemoglobin is lower for 970 nm lasers than for an 800 nm laser, absorbance by oxygenated hemoglobin is similar for both wavelengths, and light scattering in breast tissue is lower for 970 nm lasers compared to 800 nm lasers.[57] However, in clinical practice, lasers from 800 to 980 nm perform similarly with regard to heat generation and light penetration.[58] Thus other types of lasers and different wavelengths could also be used for excitation of Pab-MWCNTs to achieve similar results to those described in our study. The temperature achieved by laser based thermotherapy is determined by the rate and quantity of energy delivery, and the efficiency of conversion of light into heat. In the clinic, laser powers ranging from 2 to 30 W, and treatment times from a few min to more than 20 min are typically employed.[4] Thus, the experimental conditions selected are consistent with current clinical practice. NIR exposure of tumors that contain MWCNTs leads to higher peak temperature and a more homogenous distribution of ablative temperatures throughout the tumor lesion and minimizes collateral damage to surrounding normal cells and tissues because of thermal diffusion.[59] In the future, it may be possible to localize NP heating to individual cells under some conditions,[60–63] but the necessary lasers are not currently available for routine clinical use.

The toxicity profile of CNTs is dependent upon the physicochemical characteristics of the specific particles.[64] For example, toxicity tests involving very long, pristine CNTs similar to raw material used for industrial purposes demonstrate the potential carcinogenicity of CNTs in some models,[65] but not in others.[66] In addition to the heterogeneity of CNT physicochemical characteristics used in various different studies, there are many other factors that prevent a comprehensive understanding of CNT toxicity. We previously observed that the toxicity of DSPE-PEG coated MWCNTs differs between treatments of cells grown on plastic versus on extracellular matrix, and between cells grown as monolayers versus 3D spheroids.[39] Moreover, *in vitro* measures of potential *in vivo* toxicity such as thrombogenicity are not necessarily predictive of actual *in vivo* responses to various types of MWCNTs.[67] Thus, in addition to particle-specific properties, cell type, culturing conditions, and whether studies were performed *in vitro* or *in vivo* can influence the toxicity profile of CNTs. Furthermore, it is important to differentiate between the confounding results of toxicity assessments designed to determine the effect of accidental or environmental exposure to unmodified CNTs from tests involving intentional exposure to CNTs which have been modified for biomedical applications.[68] Nonetheless, our previous studies show the safety of local or systemic administration of CNTs in rodents[20–22,28,67] and recent studies by others show the safety of intravenously injected CNTs in nonhuman primates.[69] Taken together, these studies provide strong support that proper functionalization

of CNT surfaces, which includes the strategy we have used in this work, can render CNTs safe for future use in humans.

We and others have shown that CNTs can effectively be delivered to tumors in mice by intravenous injection.[10,21,37] Furthermore, we recently showed that our Pgp antibody can effectively target Pgp-expressing tumors *in vivo*.[38,70] Therefore, we believe that in the near future, Pgp targeting will enhance the delivery of MWCNTs to tumor sites, especially drug-resistant tumors. Although Pab-MWCNTs may still bind to Pgp in some normal tissues or be taken up by cells and organs involved in the mononuclear phagocyte system, the tumor-directed laser irradiation will limit therapy induced toxicity to the dual laser/Pab-MWCNT targeted tumor sites.

Supplementary Material

Refer to Web version on PubMed Central for supplementary material.

Acknowledgements

This work was supported by a NIH grants R01CA194064 (X.M.) and R01CA207222 (R.S.). X. S. was sponsored by the China Scholarship Council (No: 201608440088). The authors would like to thank Dr. Michael Gottesman (NCI) for providing 3T3-MDR1 and NCI/ADR-Res cells, and Dr. Nicole Levi (Wake Forest University) for the use of the K-laser. We also acknowledge the experimental assistances of the Cellular Imaging Shared Resource and the Cell and Virus Vector Core Laboratory of the Comprehensive Cancer Center of Wake Forest Baptist Medical Center supported by a NCI grant P30CA012197.

References

1. Robey RW; Pluchino KM; Hall MD; Fojo AT; Bates SE; Gottesman MM, Revisiting the Role of ABC Transporters in Multidrug-resistant Cancer. Nat Rev Cancer 2018, 18 (7), 452–464. [PubMed: 29643473]
2. Gottesman MM; Lavi O; Hall MD; Gillet JP, Toward a Better Understanding of the Complexity of Cancer Drug Resistance. Annu Rev Pharmacol Toxicol 2016, 56, 85–102. [PubMed: 26514196]
3. Bettaieb A; Wrzal PK; Averill-Bates DA, Hyperthermia: Cancer Treatment and Beyond, Rangel Letícia, Prof. (Ed.). In Cancer Treatment - Conventional and Innovative Approaches [Online] Rangel L, Ed. InTech, 2013, 257–283.
4. Schena E; Saccomandi P; Fong Y, Laser Ablation for Cancer: Past, Present and Future. J Funct Biomater 2017, 8, 19.
5. Carpentier A; Chauvet D; Reina V; Beccaria K; Leclerq D; McNichols RJ; Gowda A; Cornu P; Delattre JY, MR-guided Laser-induced Thermal Therapy (LITT) for Recurrent Glioblastomas. Lasers Surg Med 2012, 44 (5), 361–368. [PubMed: 22488658]
6. Mohammadi A; Hawasli A; Rodriguez A; Schroeder J; Laxton A; Elson P; Tatter S; Barnett G; Leuthardt E, Laser Interstitial Thermal Therapy (Litt) as a Treatment Modality for Difficult-to-Access High Grade Gliomas: A Multi-Center Study. Neuro-Oncology 2013, 15, 221.
7. Mohammadi AM; Hawasli AH; Rodriguez A; Schroeder JL; Laxton AW; Elson P; Tatter SB; Barnett GH; Leuthardt EC, The Role of Laser Interstitial Thermal Therapy in Enhancing Progression-free Survival of Difficult-to-access High-grade Gliomas: a Multicenter Study. Cancer Med 2014, 3 (4), 971–979. [PubMed: 24810945]
8. Sloan AE; Ahluwalia MS; Valerio-Pascua J; Manjila S; Torchia MG; Jones SE; Sunshine JL; Phillips M; Griswold MA; Clampitt M; Brewer C; Jochum J; McGraw MV; Diorio D; Ditz G; Barnett GH, Results of the NeuroBlate System First-in-humans Phase I Clinical Trial for Recurrent Glioblastoma. J Neurosurg 2013, 118 (6), 1202–1219. [PubMed: 23560574]

9. Xie B; Singh R; Torti FM; Keblinski P; Torti S, Heat Localization for Targeted Tumor Treatment with Nanoscale Near-infrared Radiation Absorbers. Phys Med Biol 2012, 57 (18), 5765–5775. [PubMed: 22948207]
10. Singh R; Torti SV, Carbon Nanotubes in Hyperthermia Therapy. Adv Drug Deliver Rev 2013, 65 (15), 2045–2060.
11. Kang S; Bhang SH; Hwang S; Yoon JK; Song J; Jang HK; Kim S; Kim BS, Mesenchymal Stem Cells Aggregate and Deliver Gold Nanoparticles to Tumors for Photothermal Therapy. ACS Nano 2015, 9 (10), 9678–9690. [PubMed: 26348606]
12. Guo JF; Rahme K; He Y; Li LL; Holmes JD; O'Driscoll CM, Gold Nanoparticles Enlighten the Future of Cancer Theranostics. Int J Nanomed 2017, 12, 6131–6152.
13. Lim WQ; Gao ZQ, Plasmonic Nanoparticles in Biomedicine. Nano Today 2016, 11 (2), 168–188.
14. Bonacchi S; Cantelli A; Battistelli G; Guidetti G; Calvaresi M; Manzi J; Gabrielli L; Ramadori F; Gambarin A; Mancin F; Montalti M, Photoswitchable NIR-Emitting Gold Nanoparticles. Angew Chem Int Ed Engl 2016, 55 (37), 11064–11068. [PubMed: 27513299]
15. Zou L; Wang H; He B; Zeng L; Tan T; Cao H; He X; Zhang Z; Guo S; Li Y, Current Approaches of Photothermal Therapy in Treating Cancer Metastasis with Nanotherapeutics. Theranostics 2016, 6 (6), 762–772. [PubMed: 27162548]
16. Ijima SIT, Single-shell Carbon Nanotubes of 1-nm Diameter. Nature 1993, 363, 603–605.
17. Pantarotto D; Singh R; McCarthy D; Erhardt M; Briand JP; Prato M; Kostarelos K; Bianco A, Functionalized Carbon Nanotubes for Plasmid DNA Gene Delivery. Angewandte Chemie-International Edition 2004, 43 (39), 5242–5246. [PubMed: 15455428]
18. Singh R; Pantarotto D; McCarthy D; Chaloin O; Hoebeke J; Partidos CD; Briand JP; Prato M; Bianco A; Kostarelos K, Binding and Condensation of Plasmid DNA onto Functionalized Carbon Nanotubes: Toward the Construction of Nanotube-based Gene Delivery Vectors. Journal of the American Chemical Society 2005, 127 (12), 4388–4396. [PubMed: 15783221]
19. Lacerda L; Soundararajan A; Singh R; Pastorin G; Al-Jamal KT; Turton J; Frederik P; Herrero MA; Bao SLA; Emfietzoglou D; Mather S; Phillips WT; Prato M; Bianco A; Goins B; Kostarelos K, Dynamic Imaging of Functionalized Multi-walled Carbon Nanotube Systemic Circulation and Urinary Excretion. Adv Mater 2008, 20 (2), 225–230.
20. Singh R; Pantarotto D; Lacerda L; Pastorin G; Klumpp C; Prato M; Bianco A; Kostarelos K, Tissue Biodistribution and Blood Clearance Rates of Intravenously Administered Carbon Nanotube Radiotracers. Proc Natl Acad Sci U S A 2006, 103 (9), 3357–3362. [PubMed: 16492781]
21. Fahrenholtz CD; Hadimani M; King SB; Torti SV; Singh R, Targeting Breast Cancer with Sugar-coated Carbon Nanotubes. Nanomedicine (Lond) 2015, 10 (16), 2481–2497. [PubMed: 26296098]
22. Burke A; Ding X; Singh R; Kraft RA; Levi-Polyachenko N; Rylander MN; Szot C; Buchanan C; Whitney J; Fisher J; Hatcher HC; D'Agostino R, Jr.; Kock ND; Ajayan PM; Carroll DL; Akman S; Torti FM; Torti SV, Long-term Survival following a Single Treatment of Kidney Tumors with Multiwalled Carbon Nanotubes and Near-infrared Radiation. Proc Natl Acad Sci U S A 2009, 106 (31), 12897–12902. [PubMed: 19620717]
23. Ding X; Singh R; Burke A; Hatcher H; Olson J; Kraft RA; Schmid M; Carroll D; Bourland JD; Akman S; Torti FM; Torti SV, Development of Iron-containing Multiwalled Carbon Nanotubes for MR-guided Laser-induced Thermotherapy. Nanomedicine (Lond) 2011, 6 (8), 1341–1352. [PubMed: 21506687]
24. Santos T; Fang X; Chen MT; Wang W; Ferreira R; Jhaveri N; Gundersen M; Zhou C; Pagnini P; Hofman FM; Chen TC, Sequential Administration of Carbon Nanotubes and Near-infrared Radiation for the Treatment of Gliomas. Front Oncol 2014, 4, 180. [PubMed: 25077069]
25. Torti SV; Byrne F; Whelan O; Levi N; Ucer B; Schmid M; Torti FM; Akman S; Liu J; Ajayan PM; Nalamasu O; Carroll DL, Thermal Ablation Therapeutics based on CN(x) Multi-walled Nanotubes. Int J Nanomedicine 2007, 2 (4), 707–714. [PubMed: 18203437]
26. Zhou F; Xing D; Ou Z; Wu B; Resasco DE; Chen WR, Cancer Photothermal Therapy in the Near-infrared Region by Using Single-walled Carbon Nanotubes. J Biomed Opt 2009, 14 (2), 021009. [PubMed: 19405722]

27. Wang CH; Chiou SH; Chou CP; Chen YC; Huang YJ; Peng CA, Photothermolysis of Glioblastoma Stem-like Cells Targeted by Carbon Nanotubes Conjugated with CD133 Monoclonal Antibody. Nanomed-Nanotechnol 2011, 7 (1), 69–79.

28. Burke AR; Singh RN; Carroll DL; Wood JC; D'Agostino RB, Jr.; Ajayan PM; Torti FM; Torti SV, The Resistance of Breast Cancer Stem Cells to Conventional Hyperthermia and Their Sensitivity to Nanoparticle-mediated Photothermal Therapy. Biomaterials 2012, 33 (10), 2961–2970. [PubMed: 22245557]

29. Hleb EY; Lapotko DO, Photothermal Properties of Gold Nanoparticles under Exposure to High Optical Energies. Nanotechnology 2008, 19, 35.

30. Pedrosa P; Vinhas R; Fernandes A; Baptista PV, Gold Nanotheranostics: Proof-of-Concept or Clinical Tool? Nanomaterials (Basel) 2015, 5 (4), 1853–1879. [PubMed: 28347100]

31. Barua S; Mitragotri S, Challenges associated with Penetration of Nanoparticles across Cell and Tissue Barriers: A Review of Current Status and Future Prospects. Nano Today 2014, 9 (2), 223–243. [PubMed: 25132862]

32. Wang YC; Bahng JH; Che QT; Han JS; Kotov NA, Anomalously Fast Diffusion of Targeted Carbon Nanotubes in Cellular Spheroids. ACS Nano 2015, 9 (8), 8231–8238. [PubMed: 26181892]

33. Dhar S; Liu Z; Thomale J; Dai H; Lippard SJ, Targeted Single-wall Carbon Nanotube-mediated Pt(IV) Prodrug Delivery using Folate as a Homing Device. J Am Chem Soc 2008, 130 (34), 11467–11476. [PubMed: 18661990]

34. Marches R; Mikoryak C; Wang RH; Pantano P; Draper RK; Vitetta ES, The Importance of Cellular Internalization of Antibody-Targeted Carbon Nanotubes in the Photothermal Ablation of Breast Cancer Cells. Nanotechnology 2011, 22 (9), 095101. [PubMed: 21258147]

35. Xiao Y; Gao X; Taratula O; Treado S; Urbas A; Holbrook RD; Cavicchi RE; Avedisian CT; Mitra S; Savla R; Wagner PD; Srivastava S; He H, Anti-HER2 IgY Antibody-functionalized Single-walled Carbon Nanotubes for Detection and Selective Destruction of Breast Cancer Cells. BMC Cancer 2009, 9, 351. [PubMed: 19799784]

36. Wang CH; Huang YJ; Chang CW; Hsu WM; Peng CA, In Vitro Photothermal Destruction of Neuroblastoma Cells using Carbon Nanotubes Conjugated with GD2 Monoclonal Antibody. Nanotechnology 2009, 20 (31), 315101. [PubMed: 19597244]

37. Liu Z; Cai W; He L; Nakayama N; Chen K; Sun X; Chen X; Dai H, In Vivo Biodistribution and Highly Efficient Tumour Targeting of Carbon Nanotubes in Mice. Nat Nanotechnol 2007, 2 (1), 47–52. [PubMed: 18654207]

38. Wang M; Mao C; Wang H; Ling X; Wu Z; Li Z; Ming X, Molecular Imaging of P-glycoprotein in Chemoresistant Tumors using a Dual-Modality PET/Fluorescence Probe. Mol Pharm 2017, 14 (10), 3391–3398. [PubMed: 28813596]

39. Eldridge BN; Bernish BW; Fahrenholtz CD; Singh R, Photothermal Therapy of Glioblastoma Multiforme using Multiwalled Carbon Nanotubes Optimized for Diffusion in Extracellular Space. Acs Biomater Sci Eng 2016, 2 (6), 963–976. [PubMed: 27795996]

40. Liu Z; Tabakman SM; Chen Z; Dai H, Preparation of Carbon Nanotube Bioconjugates for Biomedical Applications. Nat Protoc 2009, 4 (9), 1372–1382. [PubMed: 19730421]

41. Ming X; Carver K; Wu L, Albumin-Based Nanoconjugates for Targeted Delivery of Therapeutic Oligonucleotides. Biomaterials 2013, 34 (32), 7939–7949. [PubMed: 23876758]

42. Yuan A; Yang B; Wu J; Hu Y; Ming X, Dendritic Nanoconjugates of Photosensitizer for Targeted Photodynamic Therapy. Acta Biomater 2015, 21, 63–73. [PubMed: 25900441]

43. Wang X; Jia G; Wang H; Nie H; Yan L; Deng XY; Wang S, Diameter Effects on Cytotoxicity of Multi-Walled Carbon Nanotubes. J Nanosci Nanotechnol 2009, 9 (5), 3025–3033. [PubMed: 19452965]

44. Burke AR; Singh RN; Carroll DL; Owen JD; Kock ND; D'Agostino R; Torti FM; Torti SV, Determinants of the Thrombogenic Potential of Multiwalled Carbon Nanotubes. Biomaterials 2011, 32 (26), 5970–5978. [PubMed: 21663954]

45. Shao N; Wickstrom E; Panchapakesan B, Nanotube-antibody Biosensor Arrays for the Detection of Circulating Breast Cancer Cells. Nanotechnology 2008, 19 (46), 465101. [PubMed: 21836232]

46. Murali VS; Wang R; Mikoryak CA; Pantano P; Draper RK, The Impact of Subcellular Location on the Near Infrared-mediated Thermal Ablation of Cells by Targeted Carbon Nanotubes. Nanotechnology 2016, 27 (42), 425102. [PubMed: 27632056]
47. Yamagishi T; Sahni S; Sharp DM; Arvind A; Jansson PJ; Richardson DR, P-glycoprotein Mediates Drug Resistance via a Novel Mechanism Involving Lysosomal Sequestration. J Biol Chem 2013, 288 (44), 31761–31771. [PubMed: 24062304]
48. Zhang P; Huang H; Huang J; Chen H; Wang J; Qiu K; Zhao D; Ji L; Chao H, Noncovalent Ruthenium(II) Complexes-Single-Walled Carbon Nanotube Composites for Bimodal Photothermal and Photodynamic Therapy with Near-Infrared Irradiation. ACS Appl Mater Interfaces 2015, 7 (41), 23278–23290. [PubMed: 26430876]
49. Park MC; Jeong H; Son SH; Kim YH; Han D; Goughnour PC; Kang T; Kwon NH; Moon HE; Paek SH; Hwang D; Seol HJ; Nam DH; Kim S, Novel Morphological and Genetic Analysis of Cancer Cells in a 3D Microenvironment Identifies STAT3 as a Regulator of Tumor Permeability Barrier Function. Cancer Res 2015 76 (5):1044–1054. [PubMed: 26676754]
50. Pattani VP; Shah J; Atalis A; Sharma A; Tunnell JW, Role of Apoptosis and Necrosis in Cell Death Induced by Nanoparticle-mediated Photothermal Therapy. J Nanopart Res 2015, 17, 1.
51. Ali MR; Rahman MA; Wu Y; Han T; Peng X; Mackey MA; Wang D; Shin HJ; Chen ZG; Xiao H; Wu R; Tang Y; Shin DM; El-Sayed MA, Efficacy, Long-term Toxicity, and Mechanistic Studies of Gold Nanorods Photothermal Therapy of Cancer in Xenograft Mice. Proc Natl Acad Sci U S A 2017, 114 (15), E3110–E3118. [PubMed: 28356516]
52. Friedrich J; Seidel C; Ebner R; Kunz-Schughart LA, Spheroid-based Drug Screen: Considerations and Practical Approach. Nat Protoc 2009, 4 (3), 309–324. [PubMed: 19214182]
53. Mehta G; Hsiao AY; Ingram M; Luker GD; Takayama S, Opportunities and Challenges for Use of Tumor Spheroids as Models to Test Drug Delivery and Efficacy. J Control Release 2012, 164 (2), 192–204. [PubMed: 22613880]
54. Madsen SJ; Sun CH; Tromberg BJ; Cristini V; De Magalhaes N; Hirschberg H, Multicell Tumor Spheroids in Photodynamic Therapy. Lasers in surgery and medicine 2006, 38 (5), 555–564. [PubMed: 16788918]
55. Li F; Zhao Y; Mao C; Kong Y; Ming X, RGD-Modified Albumin Nanoconjugates for Targeted Delivery of a Porphyrin Photosensitizer. Mol Pharm 2017, 14 (8), 2793–2804. [PubMed: 28700237]
56. Zhao Y; Li F; Mao C; Ming X, Multiarm Nanoconjugates for Cancer Cell-Targeted Delivery of Photosensitizers. Mol Pharm 2018, 15 (7), 2559–2569. [PubMed: 29764120]
57. Jacques SL, Optical Properties of Biological Tissues: a Review. Phys Med Biol 2013, 58 (11), R37–R61. [PubMed: 23666068]
58. Stafford RJ; Fuentes D; Elliott AA; Weinberg JS; Ahrar K, Laser-induced Thermal Therapy for Tumor Ablation. Crit Rev Biomed Eng 2010, 38 (1), 79–100. [PubMed: 21175405]
59. Xie B; Singh R; Torti FM; Keblinski P; Torti S, Heat Localization for Targeted Tumor Treatment with Nanoscale Near-infrared Radiation Absorbers. Phys Med Biol 2012, 57 (18), 5765–5775. [PubMed: 22948207]
60. Biris AS; Boldor D; Palmer J; Monroe WT; Mahmood M; Dervishi E; Xu Y; Li Z; Galanzha EI; Zharov VP, Nanophotothermolysis of Multiple Scattered Cancer Cells with Carbon Nanotubes Guided by Time-resolved Infrared Thermal Imaging. Journal of Biomedical Optics 2009, 14 (2), 021007. [PubMed: 19405720]
61. Zharov VP; Galitovskaya EN; Johnson C; Kelly T, Synergistic Enhancement of Selective Nanophotothermolysis with Gold Nanoclusters: Potential for Cancer Therapy. Laser Surg Med 2005, 37 (3), 219–226.
62. Vitetta ES; Marches R; Mikoryak C; Wang RH; Pantano P; Draper RK, The Importance of Cellular Internalization of Antibody-targeted Carbon Nanotubes in the Photothermal Ablation of Breast Cancer Cells. Nanotechnology 2011, 22, 9.
63. Anderson RR; Parrish JA, Selective Photothermolysis: Precise Microsurgery by Selective Absorption of Pulsed Radiation. Science 1983, 220 (4596), 524–527. [PubMed: 6836297]
64. Prato M; Kostarelos K; Bianco A, Functionalized Carbon Nanotubes in Drug Design and Discovery. Acc Chem Res 2008, 41 (1), 60–68. [PubMed: 17867649]

65. Huaux F; d'Ursel de Bousies V; Parent MA; Orsi M; Uwambayinema F; Devosse R; Ibouraadaten S; Yakoub Y; Panin N; Palmai-Pallag M; van der Bruggen P; Bailly C; Marega R; Marbaix E; Lison D, Mesothelioma Response to Carbon Nanotubes is Associated with an Early and Selective Accumulation of Immunosuppressive Monocytic Cells. Part Fibre Toxicol 2016, 13 (1), 46. [PubMed: 27549627]

66. Takanashi S; Hara K; Aoki K; Usui Y; Shimizu M; Haniu H; Ogihara N; Ishigaki N; Nakamura K; Okamoto M; Kobayashi S; Kato H; Sano K; Nishimura N; Tsutsumi H; Machida K; Saito N, Carcinogenicity Evaluation for the Application of Carbon Nanotubes as Biomaterials in rasH2 Mice. Sci Rep 2012, 2, 498. [PubMed: 22787556]

67. Burke AR; Singh RN; Carroll DL; Owen JD; Kock ND; D'Agostino R, Jr.; Torti FM; Torti SV, Determinants of the Thrombogenic Potential of Multiwalled Carbon Nanotubes. Biomaterials 2011, 32 (26), 5970–5978. [PubMed: 21663954]

68. Alshehri R; Ilyas AM; Hasan A; Arnaout A; Ahmed F; Memic A, Carbon Nanotubes in Biomedical Applications: Factors, Mechanisms, and Remedies of Toxicity. J Med Chem 2016, 59 (18), 8149–8167. [PubMed: 27142556]

69. Alidori S; Bowman RL; Yarilin D; Romin Y; Barlas A; Mulvey JJ; Fujisawa S; Xu K; Ruggiero A; Riabov V; Thorek DL; Ulmert HD; Brea EJ; Behling K; Kzhyshkowska J; Manova-Todorova K; Scheinberg DA; McDevitt MR, Deconvoluting Hepatic Processing of Carbon Nanotubes. Nat Commun 2016, 7, 12343. [PubMed: 27468684]

70. Mao C; Zhao Y; Li F; Li Z; Tian S; Debinski W; Ming X, P-glycoprotein Targeted and Near-infrared Light-guided Depletion of Chemoresistant Tumors. J Control Release 2018, 286, 289–300. [PubMed: 30081143]

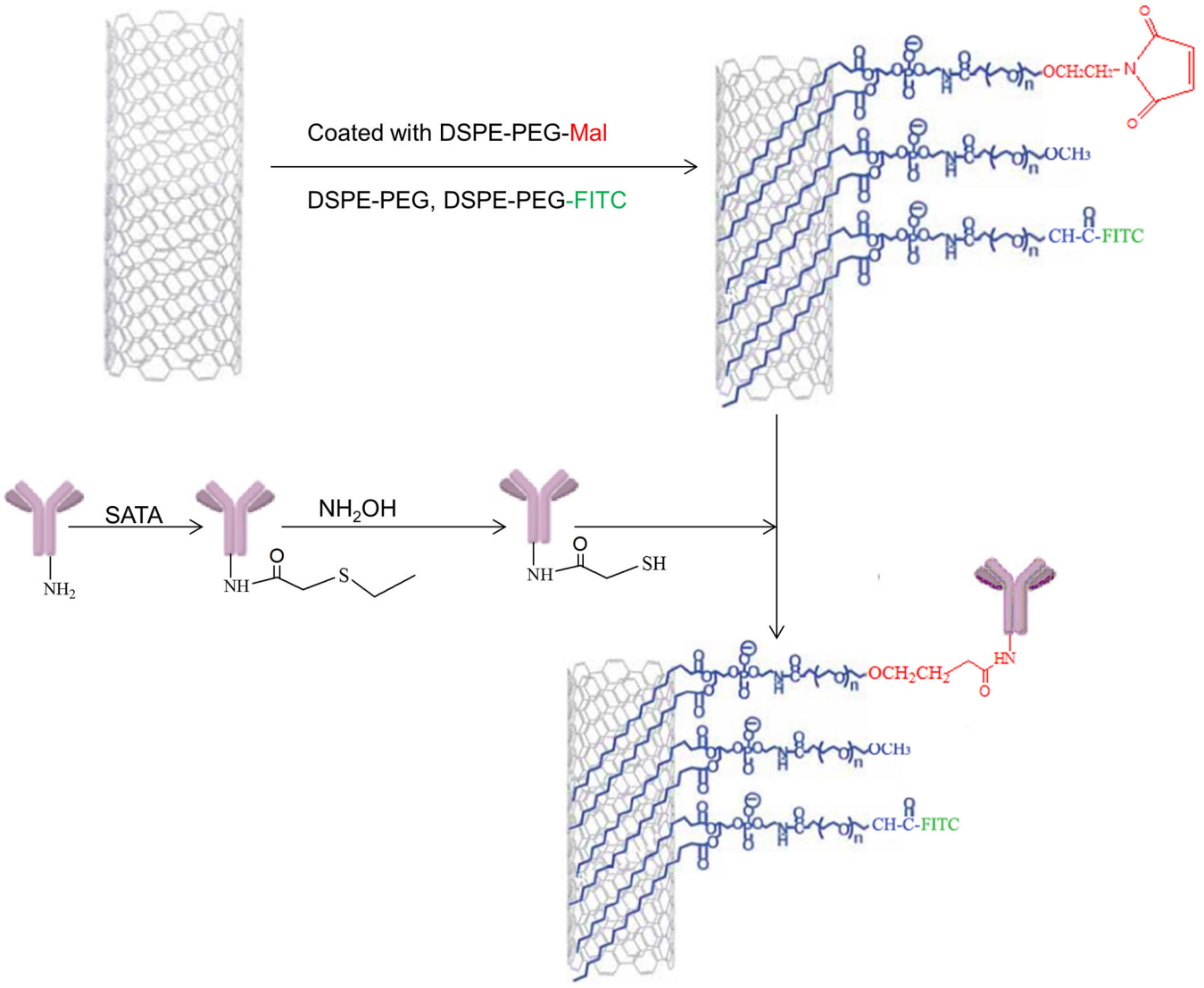

Scheme 1.
Preparation of Pab-MWCNTs

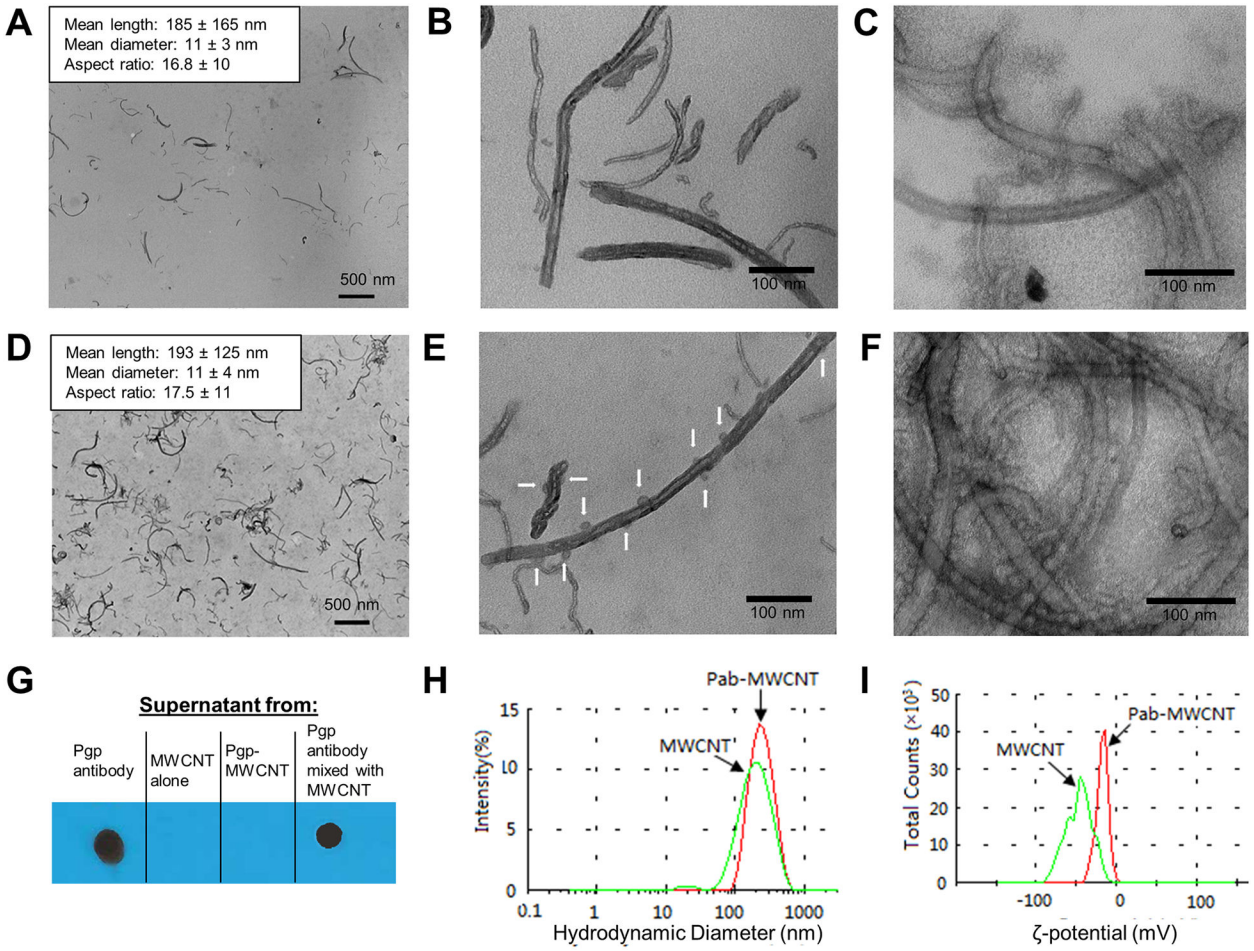

Figure 1.

Characterization of MWCNTs and Pab-MWCNTs. (A,B) Photoelectron micrographs of unstained and (C) uranyl acetate stained MWCNTs. (D,E) Photoelectron micrographs of unstained and (F) uranyl acetate stained Pab-MWCNTs. White arrows in (E) and globular masses (approx. 10 nm diameter) in (F) indicate the location of antibody molecules on MWCNTs. (G) Immunoblotting to probe for the presence of the Pab antibody with the anti-mouse secondary antibody in the supernatants of solutions containing Pab alone, MWCNT alone, freshly prepared Pab-MWCNT, and a mixture of Pab with MWCNT. (H) Hydrodynamic size distribution of MWCNTs and Pab-MWCNTs (red line) and MWCNTs (green line) in PBS. (I) ζ-potentials of Pab-MWCNTs (red line) and MWCNTs (green line) in water (pH 6.5).

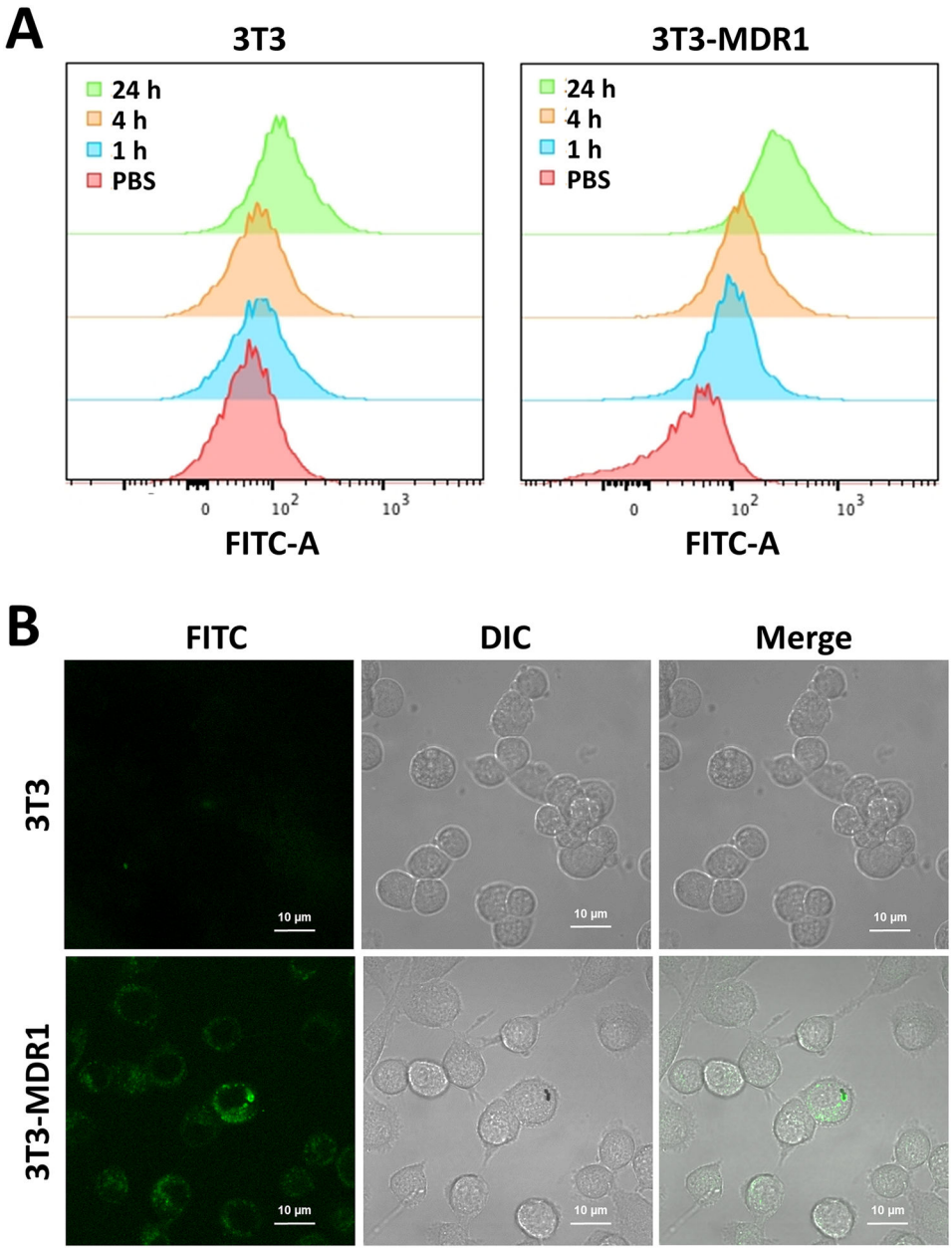

Figure 2.

Cellular uptake of Pab-MWCNTs in 3T3 cells and 3T3-MDR1 cells. A. Flow cytometry of 3T3 cells and 3T3-MDR1 cells after treating with FITC-labeled Pab-MWCNTs at 10 μg/mL for 1, 4, and 24 h. B. Intracellular distribution of FITC labelled Pab-MWCNTs at 10 μg/mL in 3T3 and 3T3-MDR cells after 4-h incubation.

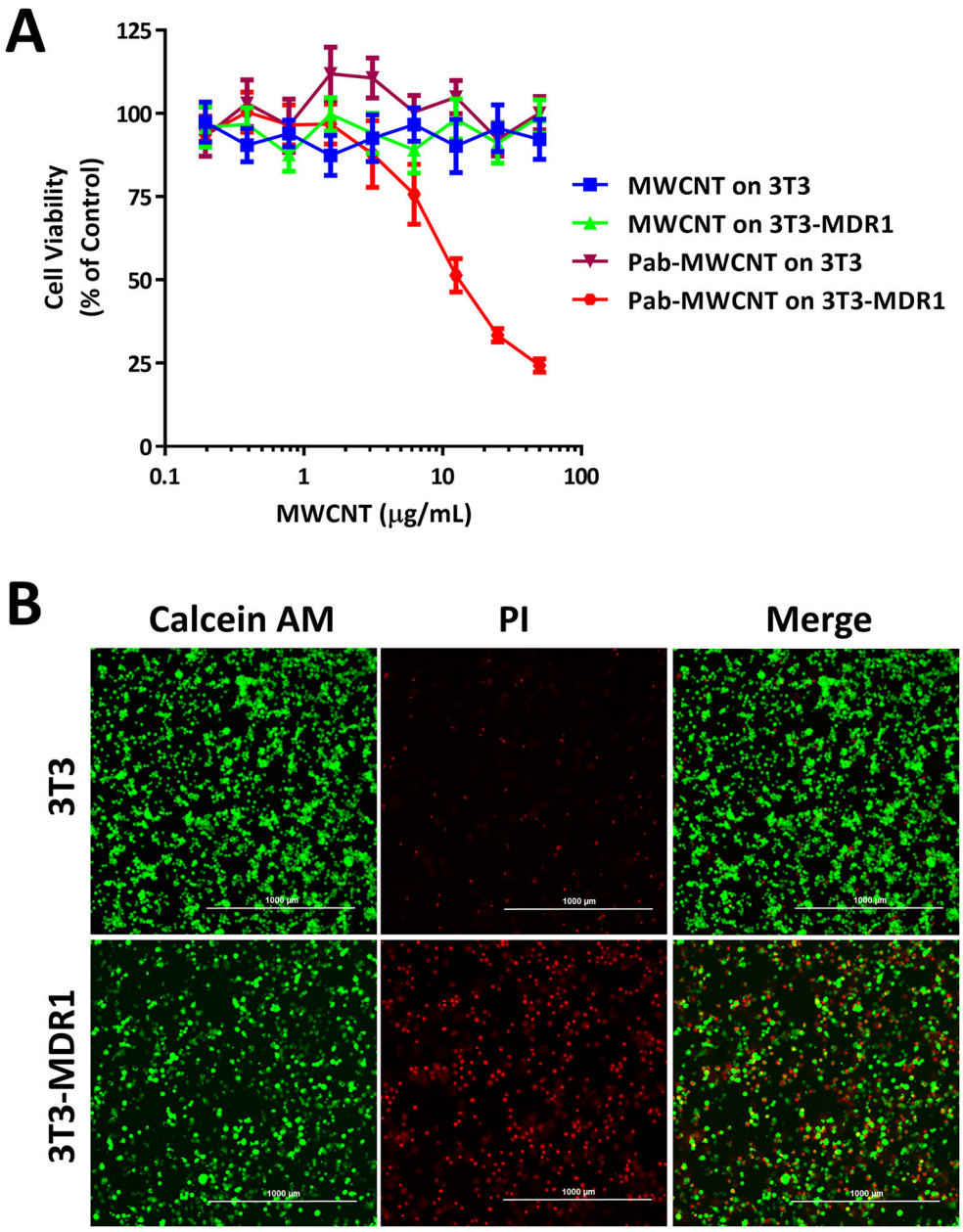

Figure 3.

Phototoxicity of Pab-MWCNTs in 3T3 and 3T3-MDR1 cells. (A) Cells were treated with Pab-MWCNTs or MWCNTs at different concentrations for 1 h before irradiation for 45 s. Alamar Blue assay was performed to measure cell viability. (B) Live/dead cell staining of 3T3 and 3T3-MDR1 after targeted PTT. Cells were treated with the Pab-MWCNTs at 10 μg/mL for 1 h. Live/dead cell staining was performed after the cells were irradiated for 45 s.

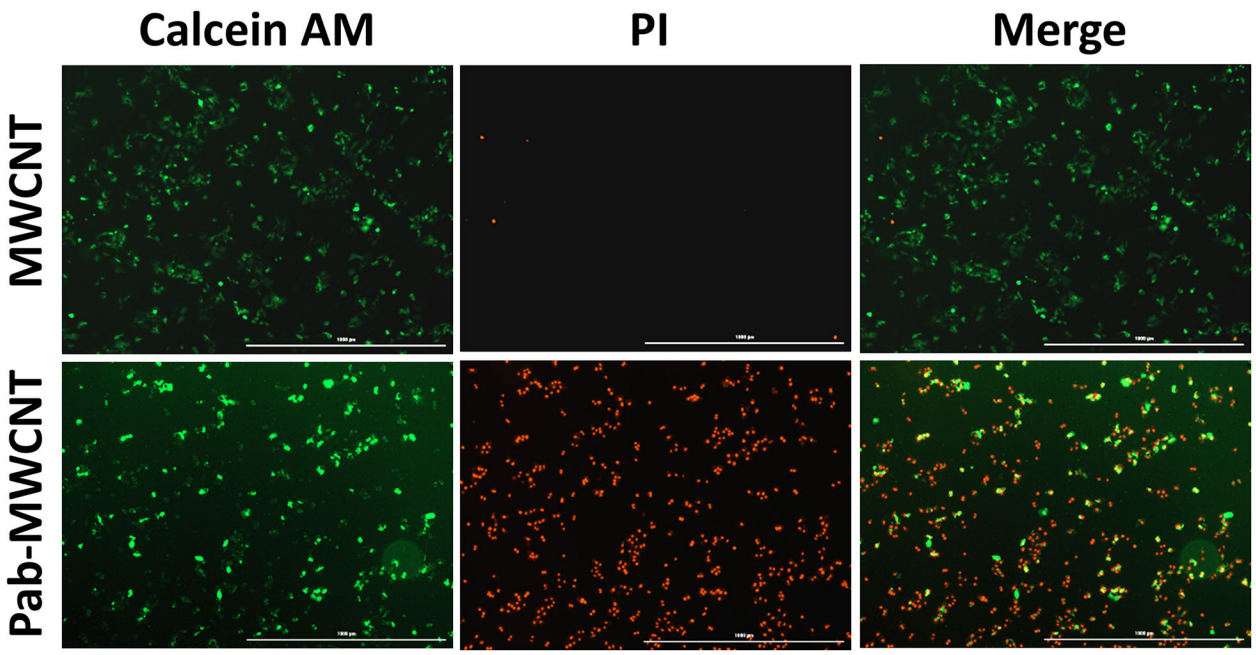

Figure 4.

Phototoxicity in NCI/ADR-RES cells. NCI/ADR-RES cells were treated with the MWCNTs or Pab-MWCNTs for 1 h. Live/dead cell staining was performed after the cells were irradiated for 45 s.

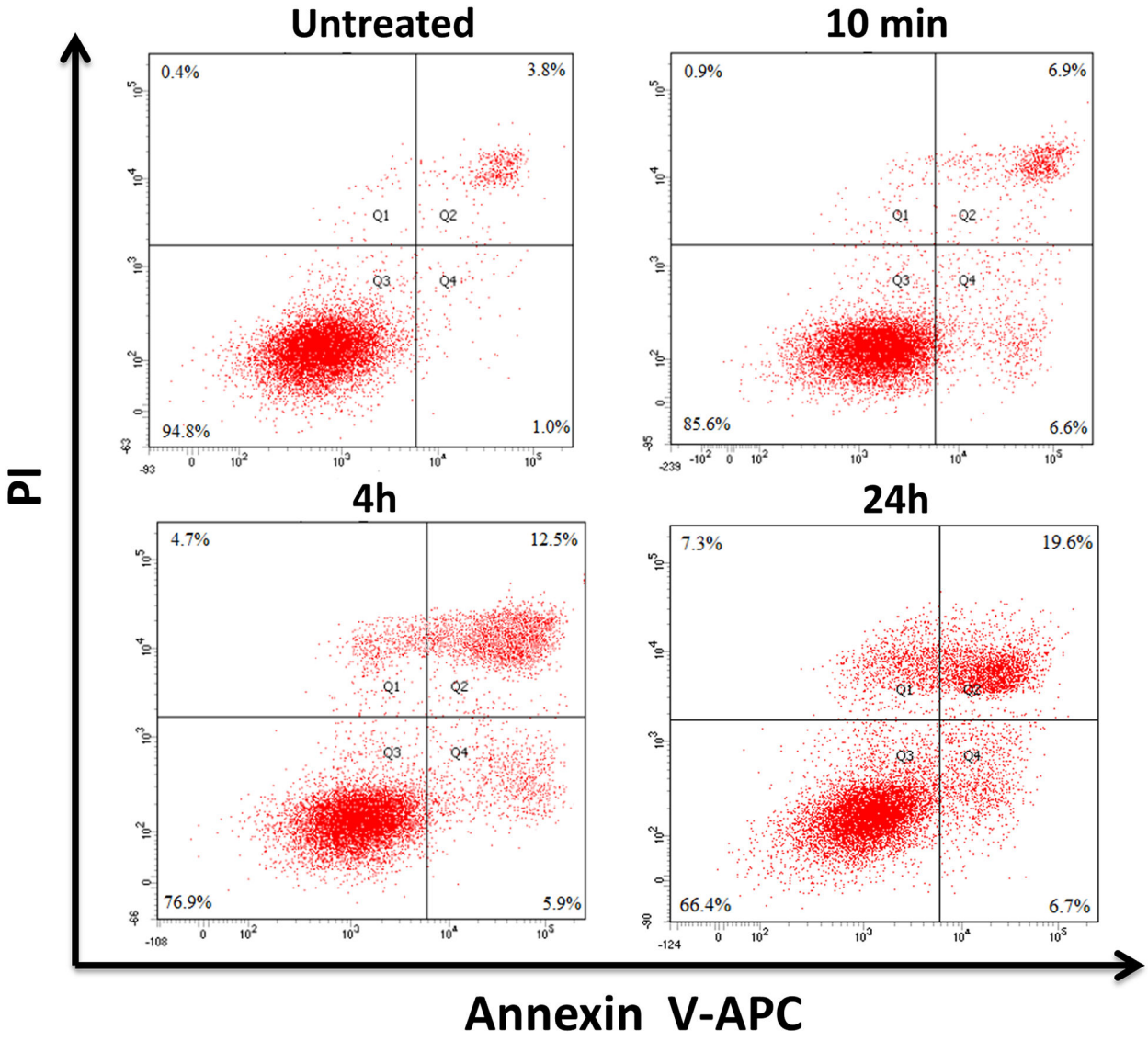

Figure 5.

Flow cytometry analysis of death pathways following Pab-MWCNT-mediated PTT. NCI/ADR-RES cells were treated with Pab-MWCNTs at 10 μg/mL for 1 h and irradiated with the K-laser. Analysis was performed at the indicated time points.

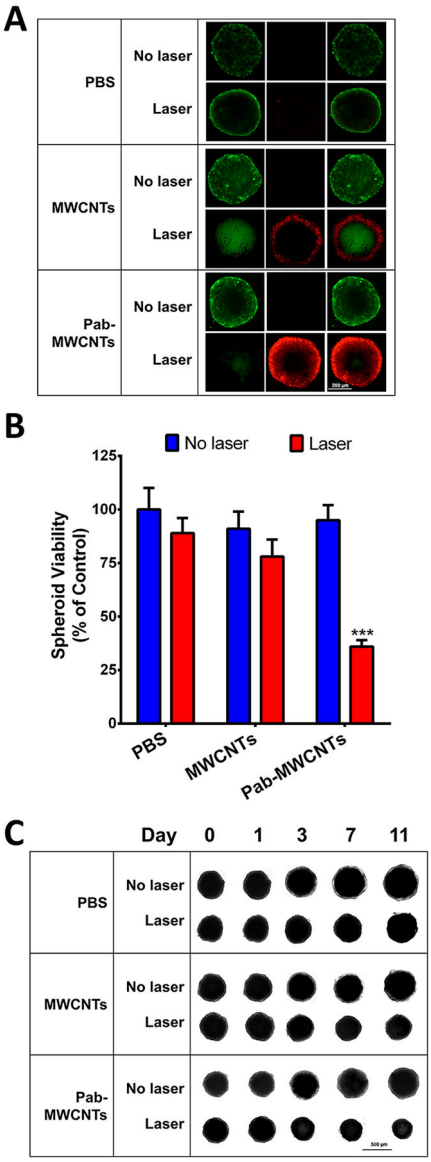

Figure 6.

Phototoxicity of Pab-MWCNTs on NCI-ADR/RES cells grown as multicellular spheroids. Tumor spheroids were treated with MWCNTs or Pab-MWCNTs at 25 μg/mL for 1 h, then exposed to the NIR laser for 45 s. (A) Live/dead cell staining with Calcein AM and PI in NCI-ADR/RES spheroids was performed one day after irradiation. (B) Alamar Blue assay of NCI-ADR/RES spheroids was performed one day after irradiation to quantify the phototoxicity. (C) The spheroids were imaged after treatments to monitor their growth over time.